Transport Behavior of Multimetallic Ultradispersed Nanoparticles in an Oil-Sands-Packed Bed Column at a High Temperature and Pressure

ARTICLE *in* ENERGY & FUELS · FEBRUARY 2012

Impact Factor: 2.79 · DOI: 10.1021/ef201939f

3 AUTHORS, INCLUDING:

Nashaat N Nassar
The University of Calgary
65 PUBLICATIONS **887** CITATIONS

SEE PROFILE

energy&fuels

Article

pubs.acs.org/EF

Transport Behavior of Multimetallic Ultradispersed Nanoparticles in an Oil-Sands-Packed Bed Column at a High Temperature and Pressure

Rohallah Hashemi, Nashaat N. Nassar,* and Pedro Pereira-Almao

Department of Chemical and Petroleum Engineering, University of Calgary, 2500 University Drive Northwest, Calgary, Alberta T2N 1N4, Canada

ABSTRACT: Water-in-vacuum gas oil microemulsion containing ultradispersed multimetallic colloidal nanoparticles can facilitate *in situ* delivery of nanoparticles into a heavy oil reservoir. This study investigated the transport of multimetallic nanoparticles (W, Ni, and Mo) of potential catalytic value suspended in vacuum gas oil using different oil-sands-packed bed column breakthrough experiments at a typical pressure and temperature of the steam-assisted gravity drainage (SAGD) recovery process. The nanoparticles (34 ± 0.5 nm) were transported into two different permeability oil sands. Experiments were performed at a pressure of 3.5 MPa, residence time of 36 h, and temperatures from 300 to 320 °C in both low- and high-permeability-oil-sands-packed beds. At full breakthrough, a constant normalized concentration plateau was achieved, ranging from 0.50 for low-permeability oil sands to 0.60 for high-permeability oil sands. Deposition and transport of nanoparticles were strongly dependent upon their metallic type, temperature, and porosity of oil sands. Despite aggregation of nanoparticles at a high temperature, neither major permeability reduction nor pore plugging were observed. Therefore, propagation of multimetallic ultradispersed nanoparticles in oil sands media seems feasible under a typical pressure and temperature of the SAGD process.

1. INTRODUCTION

The worldwide global demand for oil has recently grown to 80 million barrels/day and is estimated to grow by 50% in the next 20 years, while conventional resources are declining.[1] Alternative energy resources will ultimately be required to sustain industrial activities, but immediate needs require a greater recovery of the unconventional resources. Heavy oil and bitumen have been considered as a long-term replacement for conventional resources.[2] However, the current technologies for upgrading heavy oil/bitumen are more complex than the technologies used for conventional crude oil. Actually, the current heavy oil recovery and upgrading processes face a number of environmental challenges.[3] These challenges stem from the large amounts of energy and water required for production and upgrading processes and the large amounts of solid waste, wastewater, and gaseous emissions that are generated.[4] Nonetheless, several research projects have been conducted to reduce the environmental footprint of the oil sands industry and to improve the quality of produced oil with cost-effective and environmentally friendly techniques.[4−15] *In situ* upgrading of heavy oil and bitumen using ultradispersed (UD) nanoparticles is a promising technology, aiming at improving the quality of produced liquids with less environmental impact. In this process, hydrogen and nanoparticle suspension could be injected into the reservoir during the steam-assisted gravity drainage (SAGD) or thermal recovery process. It is believed that nanoparticles combined with the SAGD process will upgrade the heavy oil within the reservoir, whereupon light oil comes to the surface and waste hydrocarbons, solids, and minerals stay subsurface.[4]

One important step in this proposed *in situ* upgrading process is the placement of the nanoparticles deep underground to provide a reaction between co-reactants without major formation damage or pore plugging. In fact, *in situ* catalytic upgrading using nanoparticles is a relatively new field of interest, and consequently, there is very little research published on the issue of nanoparticle propagation inside the oil sands medium at recovery or upgrading conditions. Most of the studies pertaining to the transport behavior of the nanoparticles in porous media are mainly focused on deep bed filtration for wastewater treatment, and the obtained results could not be applied for reaction conditions in the oil-based matrix.[16−18] Nonetheless, our research group has recently reported on the transport of suspended UD catalysts in the heavy oil matrix at a low temperature through oil sands media and in the absence of any chemical reaction.[9−11] Results demonstrated that it is feasible to propagate UD nanoparticles in oil sands media without major permeability reduction and significant pressure drop. It was found that the sand media, mainly at the bed entrance, retained 14−18% of injected UD nanoparticles.

This study is actually a continuation on our previous work aiming at experimentally investigating the transport behavior of nanoparticles in an oil sands porous media at high pressure and temperature of SAGD conditions. The specific objectives are to test (i) the transport, deposition, and retention of multimetallic nanoparticles through one-dimensional (1D) column experiments with two different model permeabilities and (ii) the effects of the temperature on the transport behavior of nanoparticles. This work will give insight into the transport

Received: December 9, 2011
Revised: February 14, 2012
Published: February 14, 2012

   dx.doi.org/10.1021/ef201939f | *Energy Fuels* 2012, 26, 1645−1655

behavior of nanoparticles in the presence of the reaction in an oil sands matrix and help in finding the best way of placing these nanoparticles in the oil reservoir for the petroleum industry. The selected metal nanoparticles are commonly used as catalysts in the petroleum industry. To the best of our knowledge, a study on the transport of multimetallic nanoparticles in an oil-sands-packed bed column at a high temperature and pressure is conducted for the first time. It should be noted that a later study would consider the employment of the transported nanoparticles for catalytic heavy oil upgrading in an oil-sands-packed bed.

2. MATERIALS AND METHODS

2.1. Chemicals. Sand-packed bed preparation was performed using silica sand as porous media (99% of SiO_2, AGSCO, Hasbrouck Heights, NJ). Athabasca bitumen (JACOS, Alberta, Canada) was used as a source of heavy oil to saturate the porous media. Vacuum gas oil (VGO, Nexen, Alberta, Canada) was used as the oil medium for nanoparticle suspension and carrier for the stabilized nanoparticles.

Table 1. Properties of Athabasca Bitumen and Nexen VGO Considered in This Study

property	bitumen	VGO	
viscosity at 40 °C (cP)	7550		122.314
API gravity (deg)	9.5		19.1
microcarbon residue (wt %)	12		NA[a]
H/C (atomic ratio)	1.52 ± 0.001		NA
sulfur (wt %)	4.25		2.73
distillation cuts (wt %)		distillation cuts (wt %)	
naphtha: IBP−213 °C	2.76 ± 0.29	IBP−235 °C	10.92
distillates: 213−343 °C	14.89 ± 0.81	235−280 °C	7.97
VGO: 343−545 °C	34.68 ± 1.81	280−343 °C	16.60
residue: >545$^+$ °C	47.95 ± 1.57	residue: >343$^+$ °C	64.51

[a]NA = not available.

Table 1 shows the properties of Athabasca bitumen and Nexen VGO. The following metal precursors were used to prepare the corresponding metal oxide nanoparticles in the VGO matrix, namely, nickel acetate tetrahydrate (99%, Sigma-Aldrich), ammonium metatungstate (99%, Sigma-Aldrich), and ammonium molybdate tetrahydrate (99%, Sigma-Aldrich). Nitric acid (70%, Sigma-Aldrich) and phosphoric acid (85%, Sigma-Aldrich) were used as digesting agents for oil sands containing metal oxide nanoparticles for metal analysis.

2.2. Porous Media. Two model porous media were selected for column breakthrough experiments, including clean unconsolidated silica sands (US Sieves 12−20 and 100−140 mesh). The absolute permeability of porous media for the 12−20 mesh size was about 250 D, and the absolute permeability of porous media for the 100−140 mesh size was about 10 D. The sands were purchased from AGSCO Corporation. Before any use, the sand was washed with deionized water to remove any kind of dust or surface impurities and then was placed in a vacuum oven at 60 °C for 24 h to evaporate any remaining water. Then, the sand was transferred to a stainless-steel column for packing.

The absolute permeability of the porous media was measured by injecting water after sand packing. Water was injected inside the porous media at different rates, and two pressure transducers were used to record the pressure at injection and production points. Accordingly, the porous media permeability was estimated following Darcy's law.

2.3. Preparation of Nanoparticle Suspension. Suspension of nanoparticles in the oil matrix can be achieved using a variety of methods.[19−22] In this work, the water-in-oil (w/o) microemulsion technique was employed for *in situ* nanoparticle preparation because this system represents heavy oil matrices under SAGD conditions to a good extent.[23,24] Also, w/o microemulsion is an attractive media for nanoparticle preparation because of its ability to form and stabilize a wide variety of nanoparticles with controlled sizes.[22,25−28] The *in situ* preparation of colloidal trimetallic nanoparticles in VGO matrices followed a similar procedure developed in our previous studies.[8,29,30] In brief, an organic compound was prepared by mixing 99.57 wt % VGO and 0.43 wt % surfactant at 700 rpm and 60 °C. The mixture was stirred for about 30 min to reach stability. The surfactant was formulated in house to give a hydrophilic−lipophilic balance (HLB) of 8 by combining two commercial surfactants, namely, SPAN 80 and TWEEN-80 from Sigma-Aldrich at a ratio of 0.65:0.35 (wt/wt). An aqueous solution of the corresponding metal salt was added to the mixture and agitated for a period of time. The total water content of the emulsions was 2.11 wt %. After that, the mixture was heated to a high temperature that was sufficient to evaporate the water and, subsequently, initiate nucleation and growth of metal oxide nanoparticles, which remain stable in suspension.[8,29,30] The total metallic concentration of the as-prepared nanoparticles was approximately 720 ppmw. The atomic metallic ratios (metal/total metal) were as follows: Mo, 0.6267; Ni, 0.1808; and W, 0.1924.

2.4. Experimental Setup. The transport behavior of nanoparticles through the oil sands porous media was investigated through a series of fixed-bed column experiments. The experimental setup is shown in

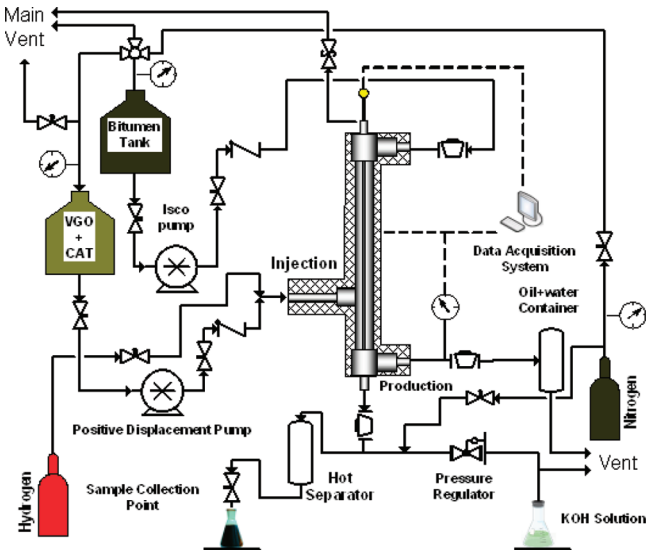

Figure 1. Schematic of the experimental setup.

Figure 1. The setup consists mainly of a VGO tank containing suspended nanoparticles under a nitrogen atmosphere, a bitumen tank under a nitrogen atmosphere, Isco pumps (Teledyne Isco, Lincoln, NE), fraction collectors, and a stainless-steel column reactor. Three Tee-shape Swagelok unions are installed at injection points, at the top and bottom of the column reactor. A hot fluid generator is connected to the top section of the oil pool (lower part of the sand-packed bed column, between the injection and production points), and a hot suspension (VGO-containing nanoparticles) was injected from this point into the porous media. It should be noted here that the injecting fluids (VGO-containing nanoparticles) were heated to the test temperature before being injected to the porous media. One 10-point thermocouple was placed in the middle of the sand-packed column all along the column reactor to record the temperature inside the porous media. Recorded temperatures were used to obtain the temperature profile distribution inside the reactor. The reactor

dx.doi.org/10.1021/ef201939f | Energy Fuels 2012, 26, 1645−1655

pressure of 3.5 MPa was maintained by a pressure regulator connected to the production line at the end of the column. Produced fluid from porous media was collected inside a hot separator of 500 cm^3 volume installed downstream and, subsequently, transferred to a sampling container for further analysis. VGO-containing nanoparticle mixtures were injected into the porous media from the injection point by a positive displacement pump. The column has a 2.16 cm inside diameter and a 90 cm height. In a certain time interval, the produced sample is collected and analyzed to measure the concentration and size of nanoparticles. Two pressure transducers were used to record the pressures of injection and production lines to calculate the pressure drop across the reaction zone.

2.5. Experimental Procedure. The experimental procedure was started with installing the packed bed reactor column in its pre-designed place in the pilot plant. In all tests, approximately 452 g of silica sand was packed in the column. Mesh rings were placed at the ends of the column to prevent sand from escaping. To ensure a uniform sand packing and to avoid air entrapment, the column was first filled with water and the sand media was introduced into the column from the top, while the column was constantly patted with a metal rod until it was fully packed. To maintain the test temperature, the outside body of the reactor column was covered with heating tapes and the column was insulated by fiberglass casing. A leak test was performed by pressurizing the packed bed reactor with pure nitrogen up to 5.5 MPa. A 1% change in pressure per hour was considered as the maximum allowable pressure reduction during the leak test. A 3.5 MPa pressure was maintained after the termination of the leak test. Nitrogen was also used for purging the system until oxygen disappeared completely, as confirmed by the gas chromatograph. After purging, the packed bed column was heated to the desired temperature. When the reactor column working pressure and temperature were attained, approximately 5 pore volumes (PVs) of bitumen were first pumped through the column in the down-flow mode to displace the water and saturated the bed with bitumen to mimic the oil sands conditions. Bitumen and irreducible water saturation were calculated by mass balance. The actual experiment started by switching the inlet gas from pure nitrogen to a hydrogen feed and introducing the injecting fluid (VGO-containing nanoparticles). At this point, the zero time for nanoparticle breakthrough was considered. The run was conducted until approximately 100 cm^3 of VGO-containing nanoparticles was injected into the porous media. Once the breakthrough experiment was complete, the reactor column was cooled to room temperature. After that, the oil sands sample was carefully discharged from the reactor column for analysis, and the column and assembly were washed with toluene; therefore, the apparatus could be ready for another cycle of experiments.

2.6. Analytical Methods. The size and concentration of the nanoparticles in the VGO matrices were measured before and after injection inside the reactor by inductively coupled plasma–atomic emission spectroscopy (ICP–AES, IRIS Intrepid II XDL, Thermo-Instruments Canada, Inc., Ontario, Canada) and dynamic light scattering (DLS, Malvern Instruments, Ltd., Worcestershire, U.K.) instruments, respectively. Before particle size measurement, about 2 drops of the produced heavy oil liquid sample containing nanoparticles were diluted with 5 mL of toluene, mixed for 1 min, and then introduced to the DLS instrument for measurement. It should be noted that a control sample (bitumen diluted in toluene) was introduced into the DLS for comparison and no significant peak was observed, indicating that the sample has no nanoparticles. Before the metal elemental analysis, the oil samples containing nanoparticles were burned at 600 °C to remove the hydrocarbons and the residue was digested with acidic solution consisting of 70% HNO_3 and 85% H_3PO_4 at a volume ratio (HNO_3/H_3PO_4) of 0.14. After that, the mixture was left shaking in a temperature incubator for 24 h at 70 °C, which was sufficient to completely dissolve the nanoparticles. To estimate the amount of nanoparticle deposited in the sand surface, the oil sands column was divided into five regions and one sample was taken from each region for metal digestion followed by ICP–AES analysis. Selected samples of deposited nanoparticles in different permeability oil sands media (obtained from the top and bottom sections of the sand-packed bed column) were analyzed by environmental scanning electron microscopy (ESEM, Philips model XL-30, Reston, VA).

3. RESULTS AND DISCUSSION

3.1. Estimating the Size of Colloidal Nanoparticles and Their Concentration in the Feed. Figure 2 shows DLS results for the sample of VGO-containing multimetallic colloidal nanoparticles of 720 ppmw at 22 °C. The average particle size diameter was about 34 ± 0.5 nm. The concentration of the colloidal nanoparticles was measured by ICP–AES, and results are tabulated in Table 2. As seen in Table 2, no significant difference is observed between nominal and experimental values of metal concentrations.

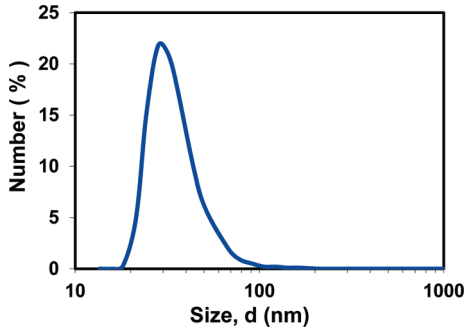

Figure 2. DLS characterization of multimetallic colloidal nanoparticle size distribution in the VGO matrix at 25 °C.

Table 2. Concentration of Multimetallic Colloidal Nanoparticles in the Feed

metal content of injecting fluid		
nominal values		experimental values
component	ppm	ppm
Ni	72	81
Mo	240	230
W	408	396
additives		
component		percentage (with respect to oil)
water (wt %)		2.11
surfactant (HLB of 8)		0.43

It should be noted that heavy oil/bitumen contains different types of metals, such as sodium, potassium, lithium, calcium, copper, iron, nickel, vanadium, manganese, etc., with nickel and vanadium being the most common metals present in the heavy oil matrix.[31] Actually, during our ICP–AES metal analysis, an appreciable amount of vanadium and nickel in the virgin bitumen matrix was observed and quantified. This explains the early breakthrough of nickel in all of the breakthrough experiments. However, the transportation behavior of injected trimetallic nanoparticles (Ni, Mo, and W) and their retention inside the porous media were the main targets of this work because of their unique catalytic properties. Thus, vanadium and other detected metals were excluded from final analysis.

3.2. Transport of Colloidal Nanoparticle in the Oil-Sands-Packed Bed Column. Because the main goal of this study was to investigate the transport behavior of the colloidal nanoparticles in the oil-sands-packed bed column, the experimental plan was designed to investigate the effect of

dx.doi.org/10.1021/ef201939f | Energy Fuels 2012, 26, 1645–1655

the temperature and permeability on the transport behavior of nanoparticles in the oil sands matrix. Table 3 shows the specifications of four breakthrough tests considered in this study. It should be noted that residence time, reactor pressure, particle concentration, and injection rates were kept fixed for all four tests.

Table 3. Specifications of the Experimental Tests Considered in This Study

properties	first test	second test	third test	fourth test
temperature (°C)	300	320	300	320
pressure (MPa)	3.5	3.5	3.5	3.5
porosity (%)	33.1	32.9	33.2	33.7
absolute permeability (D)	246.8	244	9.6	8.9
nominal particle concentration (ppm)	720	720	720	720
residence time (h)	36	36	36	36
suspension injection rate (cm^3/min)	0.01	0.01	0.01	0.01

3.3. First Test. Figure 3 shows the breakthrough curves of different nanoparticles through high permeability oil sands porous media at the experimental conditions presented in Table 3. The breakthrough curve represents the fraction of the nanoparticle concentration in the effluent fluid (C_e) from the reactor column over that in the feed (C_o) as a function of the injected fluid PV. In all cases, the effluent concentration of nanoparticles increased dramatically and rapidly reached a plateau at approximately 1.0 PV, although the levels of the plateau differed among the types of nanoparticles. This suggests that the transport and deposition behavior of the nanoparticles are affected by the type of nanoparticles but their deposition mechanism could be similar.

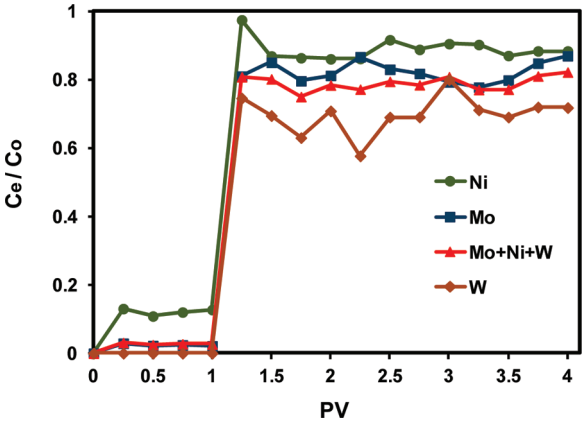

Figure 3. Breakthrough curves for experiments conducted with different nanoparticles of 34 ± 0.5 nm diameters suspended in VGO matrices in an oil-sands-packed bed column with clean silica sand of 12−20 mesh size saturated with Athabasca bitumen. Other experimental conditions include a residence time of 36 h, porosity of 33.1%, pressure of 3.5 MPa, and temperature of 300 °C.

The mass balance calculation showed that about 11 wt % Ni, 17.8 wt % Mo, and 30 wt % W inlet concentrations remained inside the oil sands porous media. This would make around 21 wt % of the total (Ni + Mo + W) nanoparticles. Nanoparticles remaining inside the oil sands porous media were either deposited on the sand grains or still suspended in the fluid remaining inside the porous media. The total amount of retained, suspended, and deposited nanoparticles was obtained from the postmortem analysis.

Table 4 shows the summary of the mass balance for the metal concentration inside the oil sands porous media. The total mass of the injected nanoparticles was calculated on the basis of the total volume of injected fluid containing nanoparticles. The total mass of produced nanoparticles (i.e., nanoparticles at the effluent of the reactor column) was estimated experimentally by ICP−AES analysis. Accordingly, the deposited and retained masses of nanoparticles in oil sands porous media were calculated from the difference between the injected and produced nanoparticles. The total mass of nanoparticles remaining suspended in the fluid (retained in the porous media) was calculated on the basis of the volume of the remaining fluid inside the porous zone. It should be noted that the concentration of nanoparticles in this fluid was estimated as the average concentration of nanoparticles in injected and produced fluids. The obtained results are tabulated in Table 4. As seen, 30.46 wt % of the injected nanoparticle concentration remained inside the oil sands column (reaction zone), among which 16.59 wt % was deposited on the sand grains. Individual and collective specific deposit trends along the reactor column of the selected nanoparticles are shown in Figure 4. This figure depicts the amount of nanoparticles (in grams) deposited per unit bed volume (in liters) of sand against the length of the reactor column (reaction zone). As seen, for all types of nanoparticles, a higher concentration was obtained at the entrance of the column, close to the injection point, although the concentration values differed among the types of nanoparticles, with Mo being the highest, followed by W and

Table 4. Mass Balance for the First Test

parameters	values
total injected nanoparticles (g)	0.0714
total produced nanoparticles (g)	0.0497
total (deposited + retained) nanoparticles (g)	0.0217
total retained nanoparticles (g)	0.0099
total deposited nanoparticles (g)	0.0119
(retained + deposited nanoparticles)/injected (wt %)	30.46
deposited nanoparticles/injected (wt %)	16.59

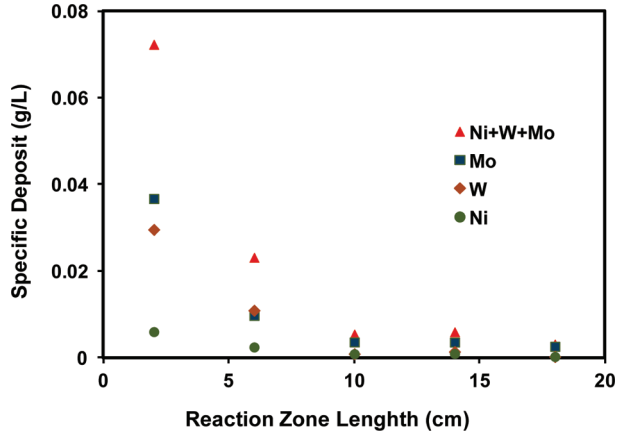

Figure 4. Calculated distribution of the specific deposit of different nanoparticles at different bed depths (across the reaction zone) for the time period of 36 h, during the run of the first test.

dx.doi.org/10.1021/ef201939f | Energy Fuels 2012, 26, 1645−1655

then Ni. This again supports the fact that the transport behavior of nanoparticles is strongly affected by the type of metal. Nonetheless, the deposition trends of the three types of nanoparticles along the reactor column were identical because all showed that retention tendency is exponentially decreased from injection to production points within the selected reaction time.

The pressure drop across the column was also measured to study the impact of nanoparticle deposition on the sand permeability. Figure 5 shows the pressure drop across the reaction zone against the PV injected. As seen in the figure, the pressure drop across the zone remained constant during the experiment. This suggests that stable experimental conditions were maintained during the test run and there was no plugging that occurred across the reaction zone. Accordingly, one can anticipate that the effect of nanoparticle injection on sand permeability reduction is meager because insignificant damage occurred on the sand-packed bed during the test. To support this conclusion, the measurement of the size of nanoparticles at different PVs was deemed necessary. Figure 6 shows DLS measurements of the particle size distribution for different PVs during this test. Clearly, no significant effect was observed on the particle size after 1.5 PV, which again supports the no plugging effect that was found by the pressure drop measurement.

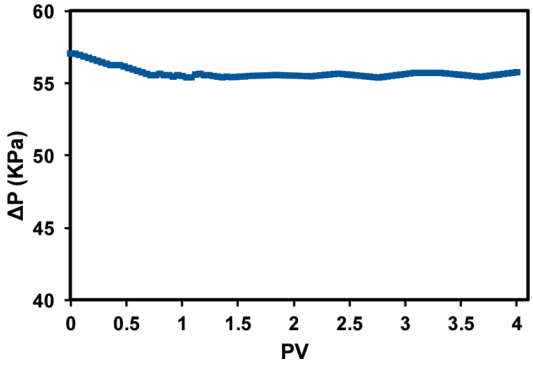

Figure 5. Pressure drop across the oil-sands-packed bed column during the run of the first test.

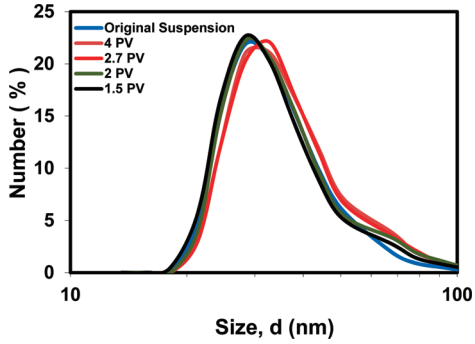

Figure 6. DLS characterization of colloidal nanoparticle size distribution in the heavy oil matrix for the original feed sample and samples obtained during the run of the first test at different values of PV.

Figure 7 shows ESEM microphotographs of two selected samples from the top and bottom of the reaction zone. Clearly, a higher population of deposited particles appeared at the top of the reaction zone compared to the bottom zone. These images support the findings obtained by the ICP–AES analysis on the trend of the specific deposit. Further, despite the aggregation of particles at the entrance of the reaction zone, still nanoparticles can propagate through the sand-packed bed column because smaller particles were observed at the production point (bottom of the column), in agreement with the DLS measurements.

3.4. Second Test. The second test has been conducted at a higher temperature to investigate the effect of the temperature on the transport behavior of nanoparticles in a high-permeability-sand-packed bed. Therefore, the experimental conditions of this test were similar to the first test, except the temperature was fixed at 320 °C. Detailed experimental conditions are shown in Table 3. Figure 8 presents the normalized breakthrough curves of produced nanoparticles against the PV. Again, for all cases, the effluent concentration of nanoparticles increased rapidly and reached a plateau at 1.0 PV, and the levels of the plateau differed among the types of nanoparticles. It is obvious that, in all cases, the level of the plateau in this test is less than the level of the plateau observed in the first test. Therefore, the total amount of remaining nanoparticles inside the porous media has been increased during this test.

Mass balance calculations showed that about 51.7 wt % W, 25 wt % Ni, and 25 wt % Mo were remaining inside the medium as either deposited on the sand grains or retained suspended inside the fluid in the porous media. The total metal concentration remaining inside the medium was 33.7 wt %, which is approximately 1.7 times higher than the amount obtained in the first test. This increase in the particle retention can be due to the increase in the particle size because of particle aggregation, which, in turn, caused pore plugging and subsequently reduced the particle transportation. Particle aggregation occurred because of the increase in the temperature, which favored particle collision because of a heavy oil viscosity reduction and subsequently higher aggregation rate.[23] This supports that the temperature plays a role on nanoparticle deposition inside the porous media. Table 5 shows the nanoparticle concentration mass balance for this test.

Qualitative behavior of the nanoparticle-specific deposit into the sand grains is depicted in Figure 9. Clearly, the concentration of nanoparticles decreased exponentially along the reaction zone, in agreement with the trend reported for the first test, within the selected reaction time. However, the retention of nanoparticles at the entrance of the reactor column is much higher than that observed in the first test. This again supports that the pore plugging has occurred because of particle aggregation. Further, the deposition of nanoparticles followed the order Mo > W > Ni, which is similar to the order observed in the first test. Figure 10 shows the particle size distribution of nanoparticle samples taken at different PVs. Clearly, the average particle size in the produced samples is greater than the average particle size in the feed. Further, no significant increase in the particle size can be observed at different values of PV, which suggests that particle aggregation had no effect on sand permeability during the residence time of this test. It should be noted that, in comparison to the first test, the size of the deposited nanoparticles in the oil sands media for this test was larger, as confirmed by ESEM measurements presented in Figure 11. This caused a slight increase in the pressure drop, as seen in Figure 12. Again, as seen in Figure 11, a high population of deposited aggregated nanoparticles appeared at the top of

dx.doi.org/10.1021/ef201939f | Energy Fuels 2012, 26, 1645–1655

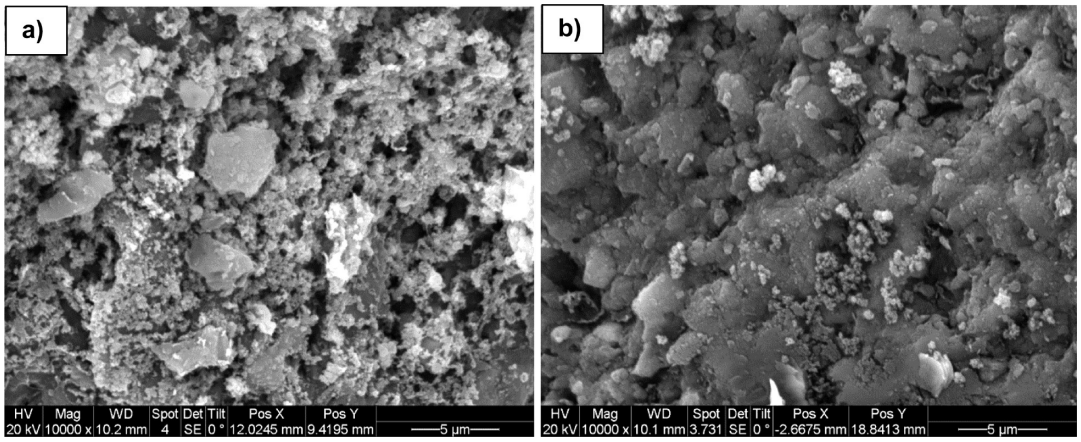

Figure 7. ESEM microphotographs of Ni–Mo–W nanoparticles deposited on high-permability oil sands porous media at the (a) top of the reactor column and (b) bottom of the reactor column. Experimental conditions include a residence time of 36 h, porosity of 32.9%, pressure of 3.5 MPa, and temperature of 300 °C.

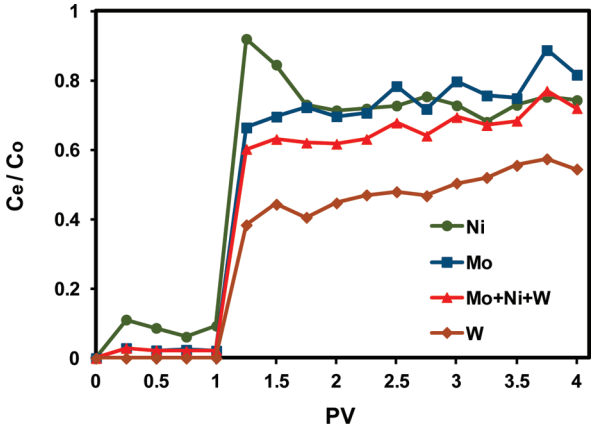

Figure 8. Breakthrough curves for experiments conducted with different nanoparticles of 34 ± 0.5 nm diameters suspended in VGO matrices in an oil-sands-packed bed column with clean silica sand of 12–20 mesh size saturated with Athabasca bitumen. Other experimental conditions include a residence time of 36 h, porosity of 32.9%, pressure of 3.5 MPa, and temperature of 320 °C.

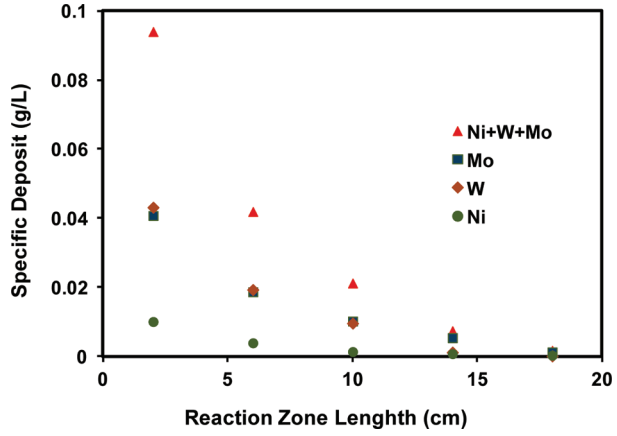

Figure 9. Calculated distribution of the specific deposit of different nanoparticles at different bed depths (across the reaction zone) for the time period of 36 h, during the run of the second test.

Table 5. Mass Balance for the Second Test

parameters	values
total injected nanoparticles (g)	0.0714
total produced nanoparticles (g)	0.0489
total (deposited + retained) nanoparticles (g)	0.0225
total retained nanoparticles (g)	0.0031
total deposited nanoparticles (g)	0.0194
(retained + deposited nanoparticles)/injected (wt %)	31.51
deposited nanoparticles/injected (wt %)	27.11

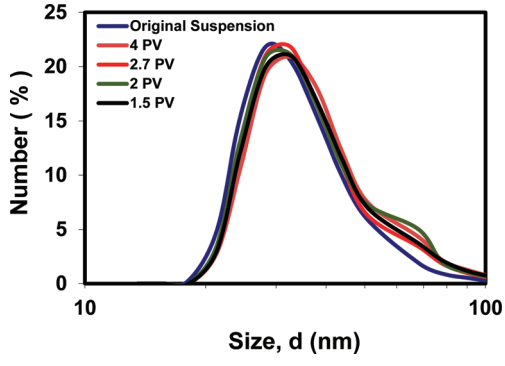

Figure 10. DLS characterization of the colloidal nanoparticle size distribution in the heavy oil matrix for the original feed sample and samples obtained during the run of the second test at different values of PV.

the reaction zone and a low population as well as smaller aggregates appeared at the bottom zone, in agreement with the ICP–AES and DLS measurements.

Figure 12 shows the pressure drop across the reaction zone against the PV. Despite a slightly higher pressure drop compared to test one, the pressure drop profile across the reaction zone remained constant throughout the experiment, which again supports that the presence of nanoparticles inside the oil sands bed has no damaging effect on the porous media.

3.5. Third Test. First and second tests have been performed in a high-permeability-oil-sands-packed bed (~245 D). However, the permeability of a typical Athabasca bitumen reservoir is much smaller.[32] To simulate the lower permeability conditions and study the effect of permeability on the transport behavior of nanoparticles, the conditions of this test run were kept similar to the conditions adopted in the first test, except that the permeability was fixed at 9.6 D (approximately 25 times less than that in the first test). Detailed experimental

dx.doi.org/10.1021/ef201939f | Energy Fuels 2012, 26, 1645–1655

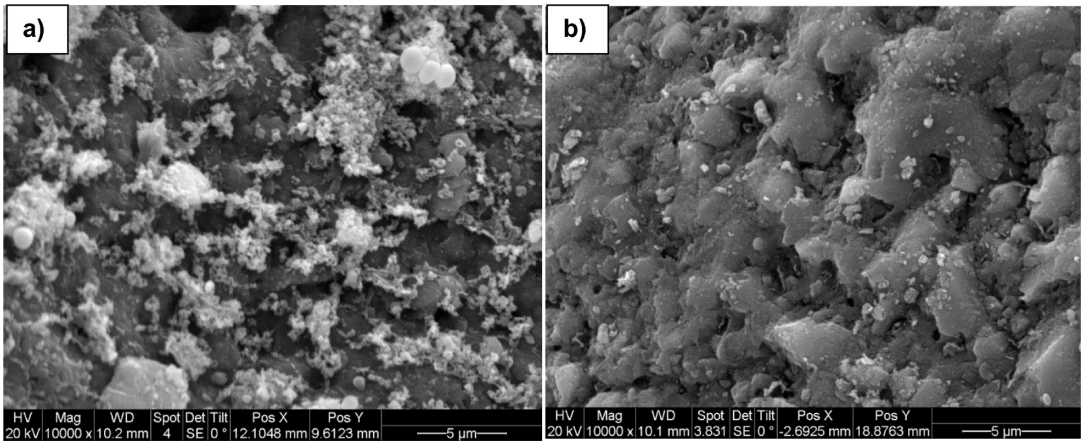

Figure 11. ESEM microphotographs of Ni−Mo−W nanoparticles deposited on high-permability oil sands porous media at the (a) top of the reactor column and (b) bottom of the reactor column. Experimental conditions include a residence time of 36 h, porosity of 32.9%, pressure of 3.5 MPa, and temperature of 320 °C.

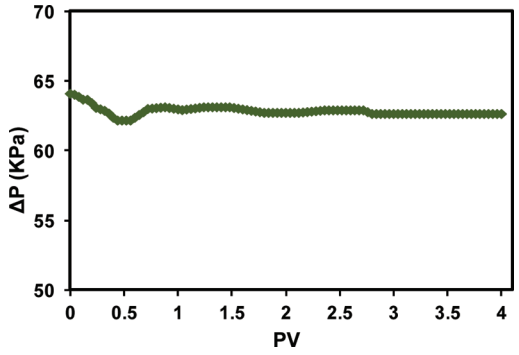

Figure 12. Pressure drop across the oil-sands-packed bed column during the run of the second test.

conditions can be seen in Table 3. Figure 13 presents the normalized breakthrough curves of produced nanoparticles against PV in a low-permeability-oil-sands-packed bed. As seen, similar to the high-permeability oil sands, after 1.0 PV of injection, metal concentrations dramatically increased and rapidly reached a plateau, but it never reached its feed concentration. Further, in all cases, the level of the plateau in the low-permeability oil sands is lower than the level of the plateau found in the high-permeability oil sands (Figure 3), suggesting that a higher amount of remaining nanoparticles inside the porous media occurred at lower permeability. Calculated values for metal concentrations showed that about 51.7 wt % W, 25 wt % Ni, and 25 wt % Mo of inlet metal concentrations remained inside the medium as either deposited or retained suspended inside the fluid in the porous media. The total amount of metal remaining in the medium was 49.35 wt %, which is much higher than that reported at high-permeability sand (first test). Also, the amount of nanoparticles deposited on sand grains was approximately 2 times higher than that for high-permeability oil sands. Detailed mass balance calculations for this test are shown in Table 6.

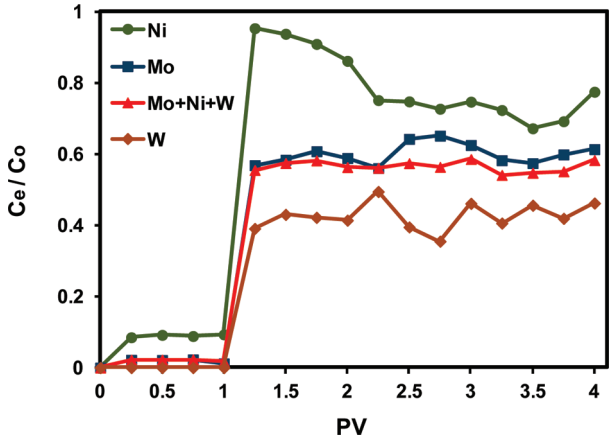

Figure 13. Breakthrough curves for experiments conducted with different nanoparticles of 34 ± 0.5 nm diameters suspended in VGO matrices in an oil-sands-packed bed column with clean silica sand of 100−140 mesh size saturated with Athabasca bitumen. Other experimental conditions include a residence time of 36 h, porosity of 33.2%, pressure of 3.5 MPa, and temperature of 300 °C.

Table 6. Mass Balance for the Third Test

parameters	values
total injected nanoparticles (g)	0.0714
total produced nanoparticles (g)	0.0362
total (deposited + retained) nanoparticles (g)	0.0352
total retained nanoparticles (g)	0.0111
total deposited nanoparticles (g)	0.0241
(retained + deposited nanoparticles)/injected (wt %)	49.35
deposited nanoparticles/injected (wt %)	33.82

Specific deposit behavior of nanoparticles on the sand surface is presented in Figure 14. As expected, a high percentage of deposited nanoparticles was located at the entrance of the reaction zone (i.e., near the injection zone). The deposition profiles for all metal nanoparticles followed the same trend of the previous tests, decreasing exponentially within the selected reaction time. However, the specific deposit value was much higher than in the high-permeability oil sands (the first test). For instance, the specific deposit at the entrance of the reaction zone in the low-permeability oil sands is approximately 2 times higher than that of the high-permeability oil sands.

It should be noted that, despite the high deposition rate of nanoparticles on sand media, no significant impact of nanoparticles on oil sands permeability could be observed. Figure 15 shows the pressure drop across the reaction zone

dx.doi.org/10.1021/ef201939f | Energy Fuels 2012, 26, 1645−1655

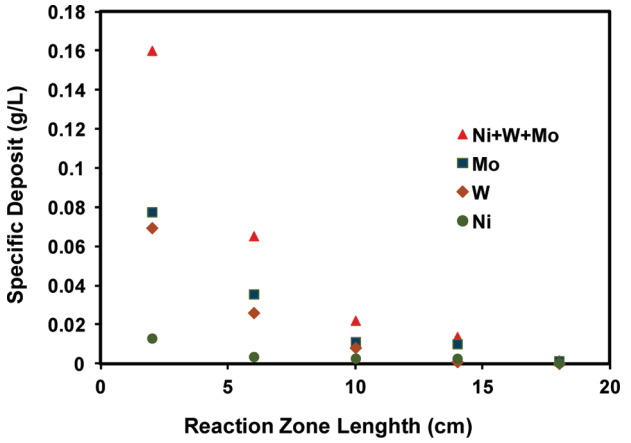

Figure 14. Calculated distribution of the specific deposit of different nanoparticles at different bed depths (across the reaction zone) for the time period of 36 h, during the run of the third test.

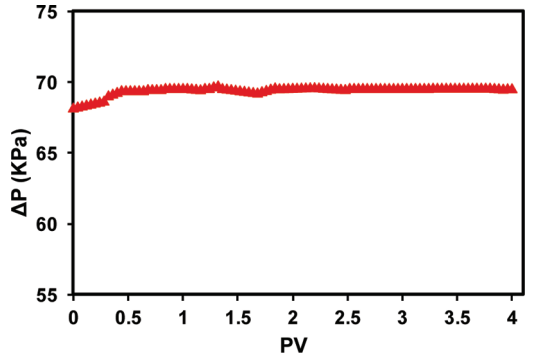

Figure 15. Pressure drop across the oil-sands-packed bed column during the run of the third test.

against PV. Except for the very early time of the test run, the pressure drop across the zone remained constant during the experiment. This suggests that a stable condition was maintained during the test run and there was no pore plugging or sand pack damage across the reaction zone. This again was supported by the DLS measurements shown in Figure 16, which represents the particle size distribution for different PVs

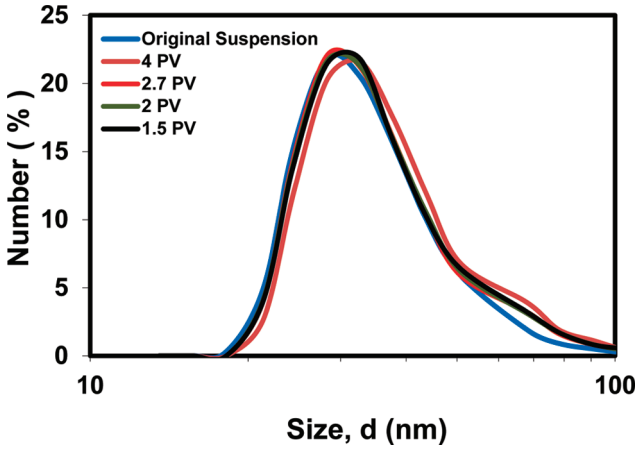

Figure 16. DLS characterization of the colloidal nanoparticle size distribution in the heavy oil matrix for the original feed sample and samples obtained during the run of the third test at different values of PV.

during this test. Similar to the other tests, the average particle size in the effluent samples was greater than the average particle size in the feed. However, clearly no significant increase in the particle size can be observed for the samples taken at different values of PV, which again suggests that particle aggregation had no effect on the oil sands permeability during the residence time of this test. It is worth mentioning that the aggregation of nanoparticles deposited on oil sand porous media in this test was greater than that found at the same temperature in the first test, as seen in Figure 17. This again supports the fact that low-permeability sand has a higher deposition rate of nanoparticles than high-permeability sand because of particle aggregation. Again, despite the high aggregation of nanoparticles at the top of the reaction zone, nanoparticles could propagate through the sand-packed bed column because smaller nanoparticles were observed at the production point, in agreement with the DLS measurements.

3.6. Fourth Test. This test was mainly performed to investigate the effect of the temperature on the transport behavior of nanoparticles in a low-permeability-oil-sands-packed bed column. Accordingly, the experimental conditions for this test were similar to the conditions reported for the third test, except that the temperature was fixed at 320 °C. Detailed experimental conditions can be found in Table 3.

Figure 18 shows the normalized breakthrough curves for different nanoparticles in a low-permeability-oil-sands-packed bed. As expected, the effluent metal concentrations increased rapidly and reached a plateau after 1.0 PV of injection. Again, the levels of the plateau did not reach the original concentration and differed among the types of nanoparticles. Further, in all cases, the level of the plateau in this test is less than the level of the plateau observed in the third test, indicating that the total amount of remaining nanoparticles inside the porous media has been increased during this test. Results of metal concentration analysis showed that 60 wt % W, 23 wt % Ni, and 44.3 wt % Mo remained inside the oil-sands-packed bed column as either deposited or remained inside the fluid in the porous media.

Table 7 shows the nanoparticle concentration mass balance in more detail. Calculation results showed that 45.13 wt % of the total injected nanoparticle concentration remained inside the medium, among which 36.11 wt % of the total concentration was deposited on the sand grains, which is slightly higher than that found in the third test. This again could be attributed to particle collision and aggregation because of the decrease in heavy oil viscosity in response to the temperature increase.

The deposition behavior of nanoparticles in this test is portrayed in Figure 19. Similarly, in all cases, exponential deposition profiles were obtained within the selected reaction time. Again, the retention of nanoparticles was much higher at the entrance of the reaction zone and declined rapidly throughout the zone length. Deposition values in this test also confirmed that the slight reduction of sand pack permeability in comparison to the third test caused a higher amount of particle retention inside the porous media.

Figure 20 shows the pressure drop profile across the reaction zone for this test. As seen, the pressure drop across the reaction zone during the test run was almost steady and constant, which suggests that no major permeability reduction or plugging during the test run occurred. As a support to this claim, DLS measurements for the particle size distribution at different PVs were performed and presented in Figure 21. Clearly, no significant change in the average particle size was observed at

dx.doi.org/10.1021/ef201939f | Energy Fuels 2012, 26, 1645–1655

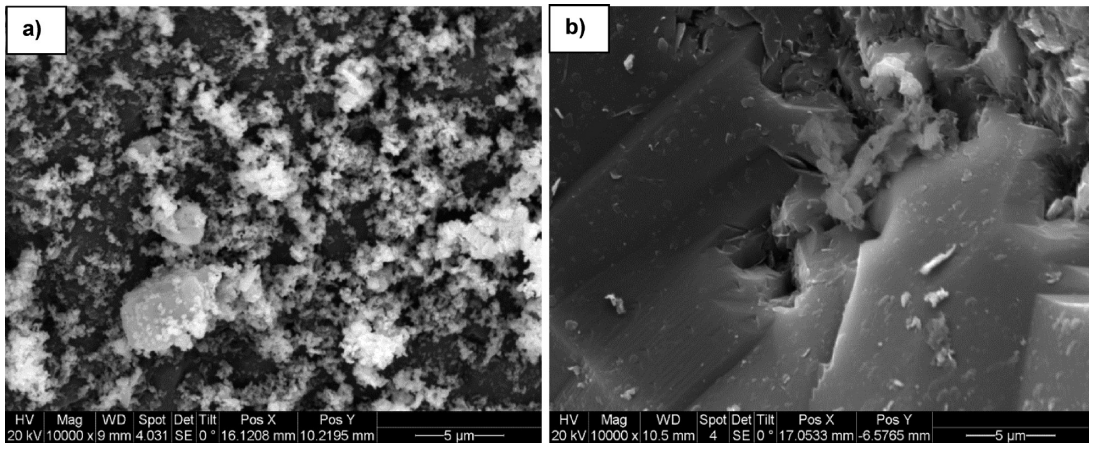

Figure 17. ESEM microphotographs of Ni–Mo–W nanoparticles deposited on low-permability oil sands porous media at the (a) top of the reactor column and (b) bottom of the reactor column. Experimental conditions include a residence time of 36 h, porosity of 33.2%, pressure of 3.5 MPa, and temperature of 300 °C.

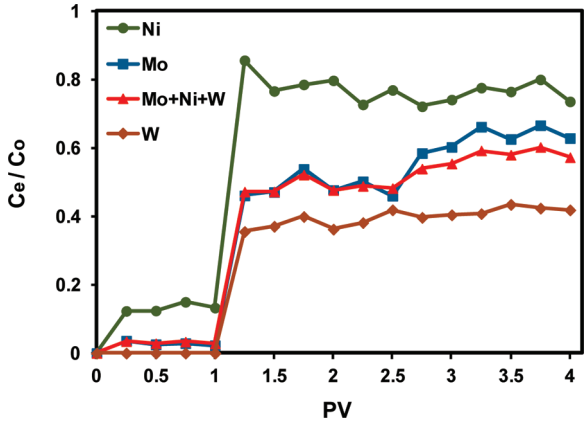

Figure 18. Breakthrough curves for experiments conducted with different nanoparticles of 34 ± 0.5 nm diameters suspended in VGO matrices in an oil-sands-packed bed column with clean silica sand of 100–140 mesh size saturated with Athabasca bitumen. Other experimental conditions include a residence time of 36 h, porosity of 33.7%, pressure of 3.5 MPa, and temperature of 320 °C.

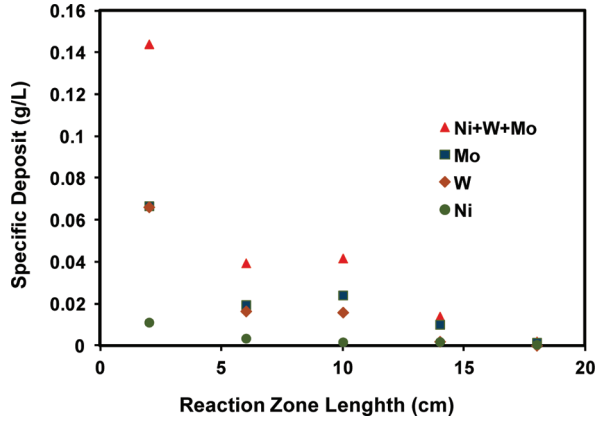

Figure 19. Calculated distribution of the specific deposit of different nanoparticles at different bed depths (across the reaction zone) for the time period of 36 h, during the run of the fourth test.

Table 7. Mass Balance for the Fourth Test

parameters	values
total injected nanoparticles (g)	0.0714
total produced nanoparticles (g)	0.0392
total (deposited + retained) nanoparticles (g)	0.0322
total retained nanoparticles (g)	0.0064
total deposited nanoparticles (g)	0.0258
(retained + deposited nanoparticles)/injected (wt %)	45.13
deposited nanoparticles/injected (wt %)	36.11

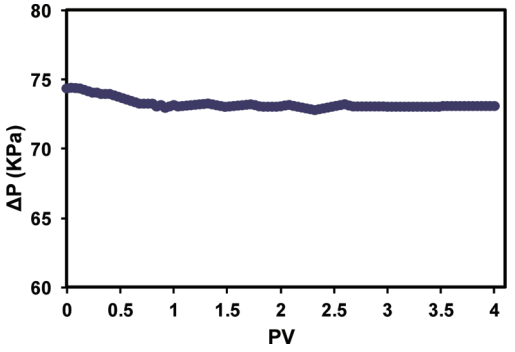

Figure 20. Pressure drop across the oil-sands-packed bed column during the run of the fourth test.

different values of PV. However, the average particle size of samples obtained in this test was higher than that obtained in the third test, suggesting that the presence of a high temperature inside the porous media favored particle aggregation, as explained earlier. This is further supported by the ESEM images shown in Figure 22.

Figure 22 shows that there is a high population of aggregated nanoparticles at the top of the reaction zone, while smaller aggregation appeared at the bottom of the reaction zone.

4. CONCLUSION

In this study, the transport behavior of UD multimetallic nanoparticles inside an oil-sands-packed bed column at a high temperature and pressure has been investigated. The stabilization of the multimetallic nanoparticles in heavy oil matrices consisting of VGO and in-house-prepared surfactants was evaluated. Column experiments were mainly conducted in this study to evaluate the transport of UD multimetallic colloidal nanoparticles in two model bitumen-saturated porous

dx.doi.org/10.1021/ef201939f | Energy Fuels 2012, 26, 1645–1655

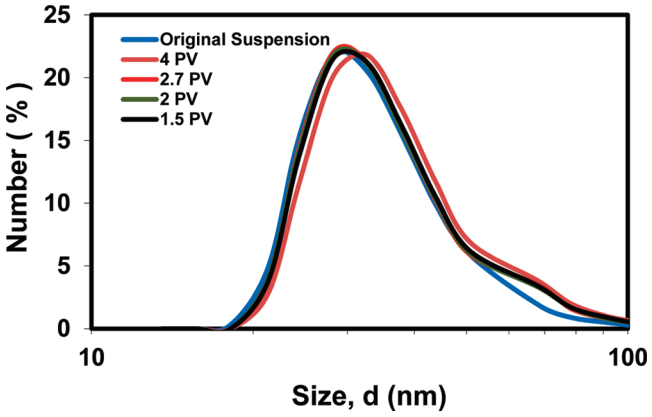

Figure 21. DLS characterization of the colloidal nanoparticle size distribution in the heavy oil matrix for the original feed sample and samples obtained during the run of the fourth test at different values of PV.

media. Particularly, different models of oil sands were employed to mimic the transport of nanoparticles in an oil reservoir during heavy oil recovery and upgrading for field application. The effect of the temperature and permeability on nanoparticle mobility in oil sands media was also evaluated. In all column experiments, aggregation of nanoparticles was observed. This was attributed to the increase in the temperature, which favored particle collision because of heavy oil viscosity reduction and, subsequently, higher aggregation rate. Results showed that a high-permeability-oil-sands-packed bed has a lower amount of deposited particles compared to the low-permeability medium. Deposition of nanoparticles mainly occurred at the entrance of the injection zone and rapidly decreased across the reaction zone. It appeared that the deposition tendency for nanoparticles is strongly affected by the type of metal, temperature, and sand permeability. Deposition of nanoparticles inside the porous media has a meager influence on medium permeability. Nonetheless, pressure drop analysis showed no major permeability damage across the reaction zone.

This study showed that UD multimetallic nanoparticles could be controllably delivered through oil sands porous media into a targeted heavy oil reservoir, where they could work as catalysts for heavy oil upgrading. The targeted transport depth can be achieved by manipulating a number of factors, such as the injection temperature, pressure, and flow rate.

AUTHOR INFORMATION

Corresponding Author

*Telephone: +1-403-210-9772. Fax: +1-403-282-3945. E-mail: nassar@ucalgary.ca.

Notes

The authors declare no competing financial interest.

ACKNOWLEDGMENTS

The authors acknowledge the Department of Chemical and Petroleum Engineering at the University of Calgary and the Alberta Ingenuity Centre for In Situ Energy (AICISE) for generously funding the project. Special thanks to Dr. Brij Maini for his beneficial comments during the experimental work, Dr. Fransisco Lopez-Linares and Lante Carbognani for their great help in the analytical work, and Redescal Gomez for preparation of nanoparticles in heavy oil matrices.

REFERENCES

(1) U.S. National Commission on Energy Policy. *Ending the Energy Stalemate: A Bipartisan Strategy To Meet America's Energy Challenges*; U.S. National Commission on Energy Policy: Washington, D.C., December 2004.

(2) National Energy Board. *Canada's Oil Sands: Opportunities and Challenges to 2015: An Update*; National Energy Board: Calgary, Alberta, Canada, June 2006.

(3) Gosselin, P. *Environmental and Health Impacts of Canada's Oil Sands Industry*; Royal Society of Canada: Ottawa, Ontario, Canada: 2010.

(4) Nassar, N. N.; Husein, M. M.; Pereira-Almao, P. *In situ* prepared nanoparticles in support of oil sands industry meeting future environmental challenges. *Explor. Prod.: Oil Gas Rev.* **2011**, *9* (1), 46–48.

(5) Galarraga, C. E.; Pereira-Almao, P. Hydrocracking of Athabasca bitumen using submicronic multimetallic catalysts at near in-reservoir conditions. *Energy Fuels* **2010**, *24* (4), 2383–2389.

(6) Hashemi, R.; Pereira-Almao, P. Experimental study of simultaneous Athabasca bitumen recovery and upgrading using ultradispersed catalysts injection. *Proceedings of the Canadian Unconventional Resources Conference*; Alberta, Canada, Nov 15–17, 2011; DOI: 10.2118/149257-MS.

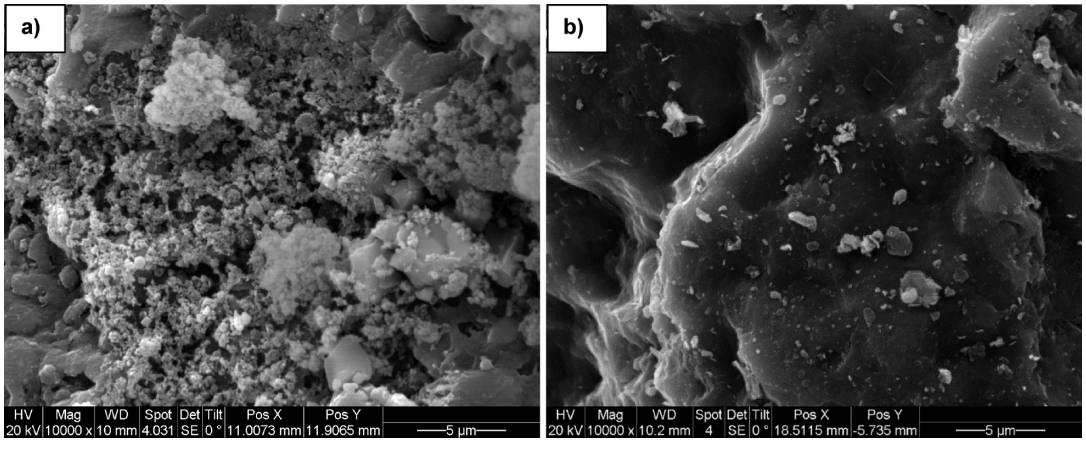

Figure 22. ESEM microphotographs of Ni–Mo–W nanoparticles deposited on low-permability oil sands porous media at the (a) top of the reactor column and (b) bottom of the reactor column. Experimental conditions include a residence time of 36 h, porosity of 33.7%, pressure of 3.5 MPa, and temperature of 320 °C.

(7) Hashemi, R.; Pereira-Almao, P. Experimental study of hot fluid injection into Athabasca oil sand reservoir. *Proceedings of the Society of Petroleum Engineers (SPE) Western North American Region Meeting*; Anchorage, AK, May 7−11, 2011; DOI: 10.2118/144558-MS.
(8) Thompson, J.; Vasquez, A.; Hill, J. M.; Pereira-Almao, P. The synthesis and evaluation of up-scalable molybdenum based ultra dispersed catalysts: Effect of temperature on particle size. *Catal. Lett.* **2008**, *123* (1), 16−23.
(9) Zamani, A.; Maini, B. Flow of dispersed particles through porous media—Deep bed filtration. *J. Pet. Sci. Eng.* **2009**, *69* (1−2), 71−88.
(10) Zamani, A.; Maini, B.; Pereira-Almao, P. Experimental study on transport of ultra-dispersed catalyst particles in porous media. *Energy Fuels* **2010**, *24* (9), 4980−4988.
(11) Zamani, A.; Maini, B.; Pereira-Almao, P. Flow of nanodispersed catalyst particles through porous media: Effect of permeability and temperature. *Can. J. Chem. Eng.* **2011**, DOI: 10.1002/cjce.20629.
(12) Nassar, N. N.; Hassan, A.; Pereira-Almao, P. Application of nanotechnology for heavy oil upgrading: Catalytic steam gasification/cracking of asphaltenes. *Energy Fuels* **2011**, *25* (4), 1566−1570.
(13) Nassar, N. N.; Hassan, A.; Pereira-Almao, P. Metal oxide nanoparticles for asphaltene adsorption and oxidation. *Energy Fuels* **2011**, *25* (3), 1017−1023.
(14) Nassar, N. N.; Pereira-Almao, P. Capturing $H_2S_{(g)}$ by *in situ*-prepared ultradispersed metal oxide particles in an oilsand-packed bed column. *Energy Fuels* **2010**, *24* (11), 5903−5906.
(15) Nassar, N. N.; Husein, M. M.; Pereira-Almao, P. Ultradispersed particles in heavy oil: Part II, sorption of $H_2S_{(g)}$. *Fuel Process. Technol.* **2010**, *91* (2), 169−174.
(16) Herzig, J.; Leclerc, D.; Goff, P. L. Flow of suspensions through porous media—Application to deep filtration. *Ind. Eng. Chem.* **1970**, *62* (5), 8−35.
(17) Rege, S.; Fogler, H. S. A network model for deep bed filtration of solid particles and emulsion drops. *AIChE J.* **1988**, *34* (11), 1761−1772.
(18) Tien, C.; Payatakes, A. C. Advances in deep bed filtration. *AIChE J.* **1979**, *25* (5), 737−759.
(19) Camacho-Bragado, G.; Elechiguerra, J.; Olivas, A.; Fuentes, S.; Galvan, D.; Yacaman, M. J. Structure and catalytic properties of nanostructured molybdenum sulfides. *J. Catal.* **2005**, *234* (1), 182−190.
(20) Afanasiev, P.; Bezverkhy, I. Synthesis of MoS_x ($5 > x > 6$) amorphous sulfides and their use for preparation of MoS_2 monodispersed microspheres. *Chem. Mater.* **2002**, *14* (6), 2826−2830.
(21) Afanasiev, P.; Xia, G. F.; Berhault, G.; Jouguet, B.; Lacroix, M. Surfactant-assisted synthesis of highly dispersed molybdenum sulfide. *Chem. Mater.* **1999**, *11* (11), 3216−3219.
(22) Eriksson, S.; Nylén, U.; Rojas, S.; Boutonnet, M. Preparation of catalysts from microemulsions and their applications in heterogeneous catalysis. *Appl. Catal., A* **2004**, *265* (2), 207−219.
(23) Nassar, N. N.; Husein, M. M. Ultradispersed particles in heavy oil: Part I, preparation and stabilization of iron oxide/hydroxide. *Fuel Process. Technol.* **2010**, *91* (2), 164−168.
(24) Husein, M. M.; Patruyo, L.; Pereira-Almao, P.; Nassar, N. N. Scavenging $H_2S_{(g)}$ from oil phases by means of ultradispersed sorbents. *J. Colloid Interface Sci.* **2010**, *342* (2), 253−260.
(25) Nassar, N. N. Study and modeling of metal oxide solubilization in (w/o) microemulsions. *J. Dispersion Sci. Technol.* **2010**, *31* (12), 1714−1720.
(26) Husein, M. M.; Nassar, N. N. Nanoparticle preparation using the single microemulsions scheme. *Curr. Nanosci.* **2008**, *4* (4), 370−380.
(27) Nassar, N. N.; Husein, M. M. Effect of microemulsion variables on copper oxide nanoparticle uptake by AOT microemulsions. *J. Colloid Interface Sci.* **2007**, *316* (2), 442−450.
(28) Nassar, N. N.; Husein, M. M. Study and modeling of iron hydroxide nanoparticle uptake by AOT (w/o) microemulsions. *Langmuir* **2007**, *23* (26), 13093−13103.
(29) Zekel', L.; Maloletnev, A.; Ozerenko, A.; Shpirt, M. Y. Basics of synthesis and application of pseudohomogeneous coal and petroleum feedstock hydrogenation catalysts. *Solid Fuel Chem.* **2007**, *41* (1), 31−37.
(30) Vasquez, A. Synthesis, characterization and model reactivity of ultra dispersed catalysts for hydroprocessing. M.Sc. Thesis, University of Calgary, Calgary, Alberta, Canada, 2009.
(31) Ovalles, C.; Rojas, I.; Acevedo, S.; Escobar, G.; Jorge, G.; Gutierrez, L. B.; Rincon, A.; Scharifker, B. Upgrading of Orinoco Belt crude oil and its fractions by an electrochemical system in the presence of protonating agents. *Fuel Process. Technol.* **1996**, *48* (2), 159−172.
(32) Akin, S.; Bagci, S. A laboratory study of single-well steam-assisted gravity drainage process. *J. Pet. Sci. Eng.* **2001**, *32* (1), 23−33.